Parameterization of Cloud Droplet Growth by Condensation

S. TRIVIKRAMA RAO[1] AND ZON-HWA FENG

Department of Atmospheric Science, State University of New York at Albany, Albany, N.Y. 12222

(Manuscript received 20 August 1976, in revised form 11 April 1977)

ABSTRACT

A parameterization scheme is developed to predict the supersaturation and the first two moments of predominantly maritime nuclei distributions during the condensation phase. The supersaturation and mean droplet growth predicted through this parameterization agree very well with those computed from the explicit microphysical equations using 55 spectral intervals.

1. Introduction

In recent years a great deal of emphasis and effort have centered around the problem of cloud droplet growth due to condensation. Models developed to simulate this process vary from complex two-dimensional models treating the microphysics explicitly (Árnason and Greenfield, 1972; Clark, 1973) to simpler models including only the bulk physics (Kessler, 1969; Árnason *et al.*, 1968). To solve the complete set of microphysical equations numerically involves the use of very small time steps, and is consequently time-consuming. The bulk-physics models, on the other hand, parameterize the condensation process in a rather crude way. It is evident from the works of Árnason and Greenfield (1972) and Silverman and Glass (1973) that considerable interactions exist between the micro- and macro-structures of cumulus clouds, particularly during early development when supersaturation plays a significant role in this interaction process. Variations in supersaturation are largely determined by the imbalance between two opposing factors: first, the adiabatic cooling due to ascending motions within the cloud which increase the supersaturation, and second, the effect of condensation which extracts the available water vapor and thereby acts to reduce the supersaturation. Furthermore, the latent heat released due to condensation, water vapor buoyancy and weight of liquid water also affect the potential temperature and vorticity distributions within the cloud. Thus, microphysical processes are inextricably coupled to macrophysical processes of hydrodynamical development on the scales of convective elements through the degree of supersaturation.

Because of the importance of the condensation process in cloud development, there is a need for a parameterization scheme that not only retains most of the properties of the explicit microphysics, but also can be economically simulated. Clark (1974) developed a parameterization scheme to predict the first three moments of the droplet distribution and supersaturation, assuming that the cloud droplet spectrum is governed by a gamma distribution, and neglecting the salt mass term (solution effect) in the droplet-growth equation. The gamma distribution for cloud droplet spectra is rather arbitrary although it may fit some observed spectra. Also, the solution effect plays a significant role in the droplet-growth equation during the initial stage of droplet growth. Therefore, the evolution of droplet growth by condensation must be examined through a cloud model including complete microphysics within a Lagrangian radius-space framework.

The objective of this paper is to present a parameterization scheme for the spectral distribution of predominantly maritime nuclei during condensational growth. The behavior of various terms in the droplet-growth equation is first explored, and from the knowledge gained a parameterization scheme is developed to predict the first two moments of the nuclei distribution, supersaturation and the total liquid water content. The results from the parameterized model are compared with those derived from the explicit microphysical computations using 55 spectral intervals. Furthermore, the usefulness of this scheme in refining the bulk-physics models is discussed qualitatively.

2. The condensation process

Prior to activation of a group of nuclei, changes in droplet radius r, in response to a change in super-

[1] Present affiliation: Division of Air Resources, New York State Department of Environmental Conservation, Albany 12233.

saturation S, are obtained by means of the equilibrium equation (Fletcher, 1966)

$$S-\frac{a}{r}+\frac{b}{r^3}=0, \tag{1}$$

such that

$$\left.\frac{dr}{dt}\right|_{\mathrm{EQU}}=\left(\frac{dS}{dt}\right)\Big/\left(\frac{3b}{r^4}-\frac{a}{r^2}\right), \tag{2}$$

where EQU stands for the equilibrium growth; $a\approx 3.3\times 10^{-5}/T$ [cm], $b=4.31im/M$ [cm^3], T is temperature, i the Van't Hoff factor, m the mass of dry salt and M the molecular weight of salt.

Once the supersaturation S reaches the droplet's critical supersaturation $S_c=2a/3r_c$ [where r_c is the critical radius given by $(3b/a)^{\frac{1}{2}}$], the growth of droplet is governed by the equation

$$(r+l)\frac{dr}{dt}=G\left(S-\frac{a}{r}+\frac{b}{r^3}\right)F,$$

where $G=D\rho_v/\rho_l(1+G_1)$, G_1 is a function depending mainly on temperature, F the ventilation factor and l a parameter inversely proportional to the accommodation coefficient.

From his experimental work, Rooth (1960) found that the value of l is less than 2 μm and suggested that it can be neglected in the droplet growth equation since its contribution to initial cloud development is limited. However, Warner's (1969) numerical computations indicated that the accommodation coefficient may account for the observed broad droplet spectrum. Our numerical experiments with Ârnason and Greenfield's (1972) two-dimensional model indicated that the accommodation coefficient does not play a significant role in the condensational growth equation. Since the measured values of the accommodation coefficient cover a wide range, it is hard to justify any specific value for it. Due to uncertainty of the role of the accommodation coefficient, we assume that it can be neglected in the droplet growth equation. The condensational growth is significant only during the initial stages of cloud development. Once the droplets have grown to a size of about 20 μm in radius, other processes such as coalescence become dominant. Fletcher (1966) suggested that for droplets <10 μm in radius, the ventilation factor is close to unity, and for droplets of 30 μm in radius its value is 1.14. Therefore, for the droplet range in which condensational growth is dominant, the ventilation effect can be neglected. With these assumptions, the droplet growth equation can be written as

$$\frac{dr}{dt}=G\left(\frac{S}{r}-\frac{a}{r^2}+\frac{b}{r^4}\right). \tag{3}$$

Eq. (3) can also be written in the form

$$\frac{dr^2}{dt}=2G\left(S-\frac{a}{r}+\frac{b}{r^3}\right) \tag{4}$$

to predict the growth rates of r^2.

The rates of growth of supersaturation and liquid water content are governed by the equations (Fletcher, 1966)

$$\frac{dS}{dt}=H_1W-H_2\frac{d\rho_w}{dt}, \tag{5}$$

$$\frac{d\rho_w}{dt}\approx 4\pi\rho_l\sum\Delta N r^2\frac{dr}{dt}, \tag{6}$$

where the summation is taken over all droplet categories. Here,

$$H_1=\frac{g}{RT_0}\left(\frac{0.622L}{C_pT_0}-1\right),$$

$$H_2=\left(\frac{L^2q_{s,0}}{C_pR_vT_0^2}+1\right)\Big/\rho_{v,s,0}.$$

For symbols not explained here, reference is made to the Appendix.

It should be recognized that the first term in Eq. (5) is a macrophysical contribution and the second term is a microphysical contribution to the changes in supersaturation. Eq. (6) can be written as

$$\frac{d\rho_w}{dt}\approx 4\pi\rho_l\left(\sum_{\mathrm{EQU}}\Delta N r^2\left.\frac{dr}{dt}\right|_{\mathrm{EQU}}+\sum_{\mathrm{NEQU}}\Delta N r^2\frac{dr}{dt}\right). \tag{7}$$

The first summation term represents the contribution from equilibrium growth [Eq. (2)] and the second from nonequilibrium (NEQU) growth [Eq. (3)].

3. Numerical results of microphysics

In order to develop a successful parameterization for the condensation process, it is necessary to understand the behavior of various terms in Eqs. (1)–(6). First of all, Eq. (3) is examined in its averaged state, i.e.,

$$\frac{\widetilde{dr}}{dt}=G\left(\frac{\tilde{S}}{r}-\frac{\tilde{a}}{r^2}+\frac{\tilde{b}}{r^4}\right), \tag{8}$$

where

$$\widetilde{(\ )}=\frac{1}{N_0}\sum_{\mathrm{NEQU}}(\ )n(r)\Delta r,$$

N_0 is the total droplet number density and the summation is taken over spectral categories which have been activated. In fact, if Eq. (8) is multiplied by N_0/N_1, N_1 being the number density of activated

TABLE 1. Data relating to the eight types of nuclei distributions used in the parameterized and microphysical models. N_0 is the cumulative number (cm^{-3}) of nuclei, K the group index, m the mass of dry salt nucleus, r_0 the droplet radius at the initial time and S_c the critical supersaturation. The Eriksson and Warner distributions are similar to those used by Årnason and Greenfield (1972). Cases 1–6 are obtained through the equation $N=CS^k$. The value of k is set 0.7 and $C=800$ for case 1, $C=1000$ for case 2 and $C=1400$ for case 3. The value of C is kept constant at 900 and $k=0.2$ for case 4, $k=0.5$ for case 5 and $k=0.9$ for case 6. Although the nuclei are initially divided into 17 groups, subsequent computations of droplet growth through explicit microphysical equations utilize 55 spectral intervals for finer resolution.

K	m (g)	r_0 (μm)	S_c (%)	N_0 Eriksson	N_0 Warner	N_0 Case 1	N_0 Case 2	N_0 Case 3	N_0 Case 4	N_0 Case 5	N_0 Case 6
1	5.80×10^{-19}	0.011	5.22600								
2	3.66×10^{-18}	0.022	2.17480	23.2690	3.236×10^{2}	1.378×10^{3}	1.723×10^{3}	2.412×10^{3}	1.051×10^{3}	1.327×10^{3}	1.811×10^{3}
3	1.46×10^{-17}	0.044	1.08950	21.8490	2.138×10^{2}	8.495×10^{2}	1.062×10^{3}	1.487×10^{3}	9.156×10^{2}	9.394×10^{2}	9.722×10^{2}
4	5.80×10^{-17}	0.085	0.54628	19.9660	1.445×10^{2}	5.239×10^{2}	6.549×10^{2}	9.169×10^{2}	7.975×10^{2}	6.652×10^{2}	5.223×10^{2}
5	2.31×10^{-16}	0.180	0.27386	17.6830	9.550×10^{1}	3.231×10^{2}	4.039×10^{2}	5.655×10^{2}	6.946×10^{2}	4.710×10^{2}	2.806×10^{2}
6	0.92×10^{-15}	0.340	0.13722	13.8220	6.310×10^{1}	1.992×10^{2}	2.490×10^{2}	3.486×10^{2}	6.050×10^{2}	3.334×10^{2}	1.506×10^{2}
7	3.66×10^{-15}	0.700	0.06877	11.4970	4.169×10^{1}	1.228×10^{2}	1.535×10^{2}	2.149×10^{2}	5.269×10^{2}	2.360×10^{2}	8.089×10^{1}
8	1.46×10^{-14}	1.080	0.03445	8.2160	2.188×10^{1}	7.570×10^{1}	9.462×10^{1}	1.325×10^{2}	4.589×10^{2}	1.670×10^{2}	4.342×10^{1}
9	5.80×10^{-14}	1.800	0.01728	5.2310	6.026	3.945×10^{1}			as in case 1		
10	2.31×10^{-13}	3.000	0.00866	2.9480	1.622	2.992			as in case 1		
11	0.92×10^{-12}	4.000	0.00434	0.9910	4.365×10^{-1}	2.270			as in case 1		
12	3.66×10^{-12}	5.000	0.00217	0.4567	1.202×10^{-1}	1.722			as in case 1		
13	1.46×10^{-11}	8.000	0.00109	0.1180	3.236×10^{-2}	1.306×10^{-1}			as in case 1		
14	5.80×10^{-11}	13.000	0.00055	0.0204	8.913×10^{-3}	9.908×10^{-2}			as in case 1		
15	2.31×10^{-10}	17.000	0.00027	0.0024	2.399×10^{-3}	7.517×10^{-3}			as in case 1		
16	0.92×10^{-9}	25.000	0.00014	0.0001	6.457×10^{-4}	5.702×10^{-4}			as in case 1		
17	3.66×10^{-9}	38.000	0.00007		1.788×10^{-4}	4.010×10^{-4}			as in case 1		

droplets, it becomes the equation of mean radius growth of activated droplets:

$$\frac{d\bar{r}}{dt}=G\left(\frac{\bar{S}}{r}-\frac{\bar{a}}{r^2}+\frac{\bar{b}}{r^4}\right), \tag{9}$$

where

$$\bar{(\ )}=\frac{1}{N_1}\sum_{\text{NEQU}}(\ )n(r)\Delta r.$$

The data used in the numerical simulation of the

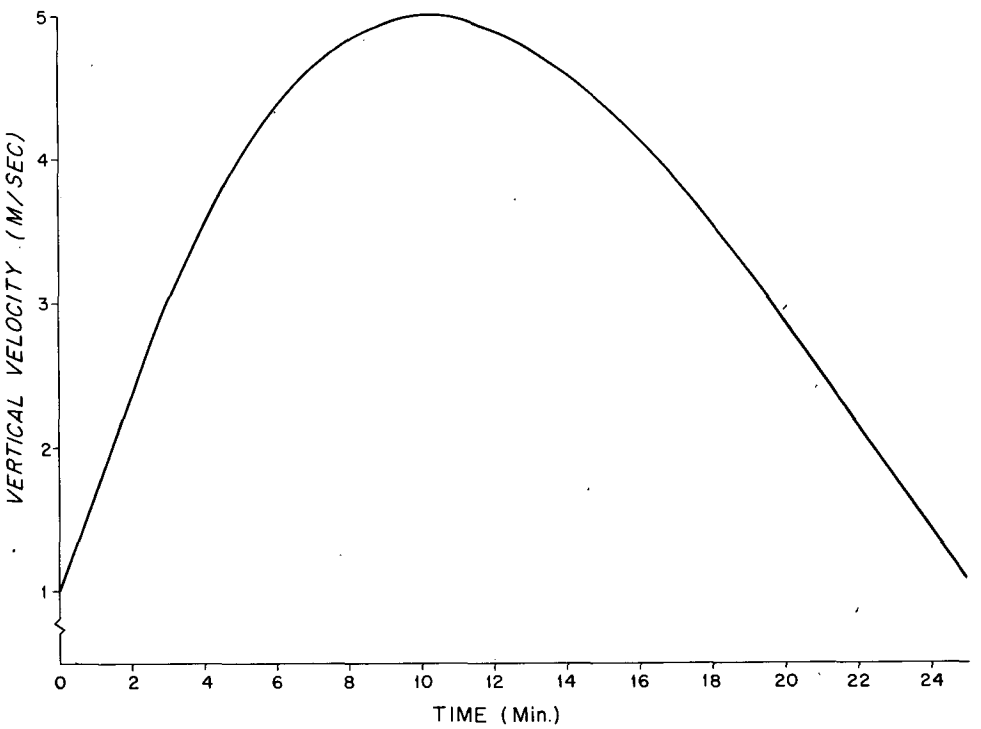

FIG. 1. Shape of the time-dependent vertical velocity used in the numerical simulations. The profile is given by $W=W_0+At-Bt^2+Ct^3$, where $W_0=1$ m s^{-1}, $A=1.481$, $B=0.1605\times10^{-2}$, $C=0.4115\times10^{-6}$, and t is time in seconds.

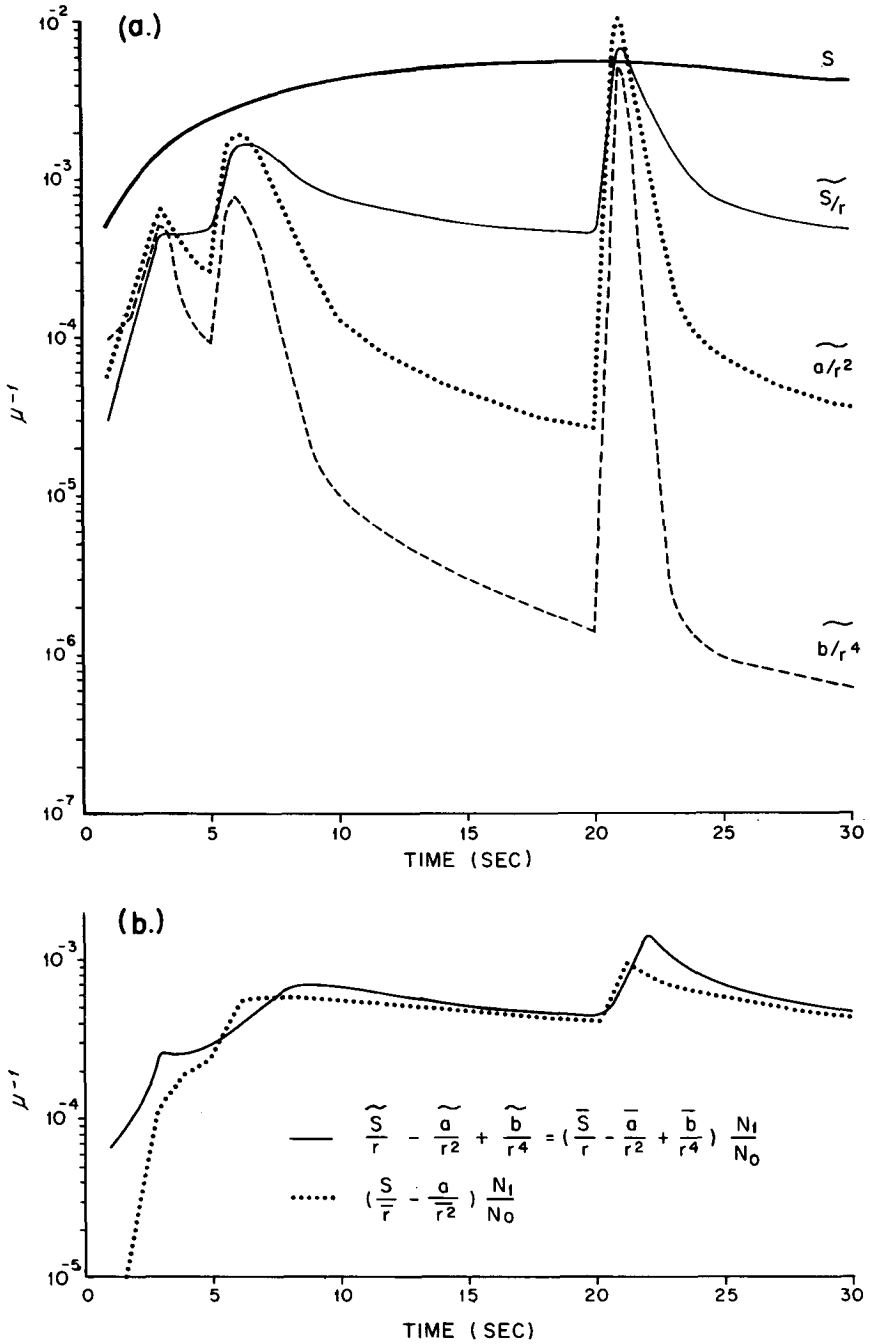

FIG. 2a. Diagram illustrating the behavior of the three terms in the mean droplet-growth equation (8). Also included for comparison is the supersaturation development derived from Eq. (5).

FIG. 2b. Comparison between terms $(S/\bar{r}-a/\overline{r^2})$ and $(\overline{S/r}-\overline{a/r^2}+\overline{b/r^4})$. Warner's nuclei distribution and a time-dependent vertical velocity are chosen for these runs.

condensation process are given in Table 1. The salt nuclei are divided into 17 groups and each is identified by its mass m; r_0 is radius of the droplet at the initial time. In subsequent computations of droplet growth, 55 spectral intervals covering a droplet radius range 0.011 to 70 μm are used for finer resolution. These data are similar to those used by Árnason and Greenfield (1972).

The droplet growth utilizing Warner's (1969) nuclei distribution is computed in the Lagrangian framework. This makes use of the fact that the number of droplets within each interval is conserved. A 1 s micro-time

step is used to ensure required accuracy and computational stability for maritime nuclei distributions (Árnason and Brown, 1971). From the macroscopic point of view, the vertical velocity W is time-dependent, and is given by $W(t)=W_0+At-Bt^2+Ct^3$, where W_0 is 1 m s^{-1}, A, B and C are constants; and t the time in seconds. This is schematically shown in Fig. 1. The vertical velocity W is changed at every macro-time step of 15 s. It is assumed that the air is saturated initially, i.e., $S_0=0$.

The behavior of the three terms in parenthesis on right-hand side of Eq. (8) for the first 30 s simulation is depicted in Fig. 2a. The development of supersaturation is also shown in the diagram for comparison purposes. The sudden jumps at 3, 6 and 21 s in the curves are due to the activation of a spectral category. This is essentially a manifestation of categorization of droplet spectra and number density in numerical treatment of the condensation process; nevertheless, the numerical results in Fig. 2a reveal that during the activation stage, the solution effect is equally as important as the other two effects. Once the activation is completed, the solution term becomes about two orders of magnitude smaller than the curvature term and three orders of magnitude smaller than the supersaturation term.

In order to investigate the relative contributions of the equilibrium growth, i.e., growth of droplets not yet activated, and solution term to the mean droplet growth, four numerical experiments are conducted: (i) a run with complete microphysics by using Eqs. (2), (3), (4), (5) and (7); (ii) a run without contribution from equilibrium growth by using Eqs. (3), (4), (5) and (7) [the $\sum_{EQU}$ term in Eq. (7) is neglected]; (iii) a run identical to (i) but neglecting solution term; and (iv) a run neglecting both equilibrium growth and solution terms.

The results of the computations of supersaturation S and mean radius $\bar{r}$ of activated droplets are shown in Figs. 3 and 4, respectively, for 10 min of simulation. It is evident from these diagrams that runs (ii)–(iv) grossly overestimate the supersaturation. The mean radius is overestimated for run (ii), while for runs (iii) and (iv) it is underestimated. The fact that

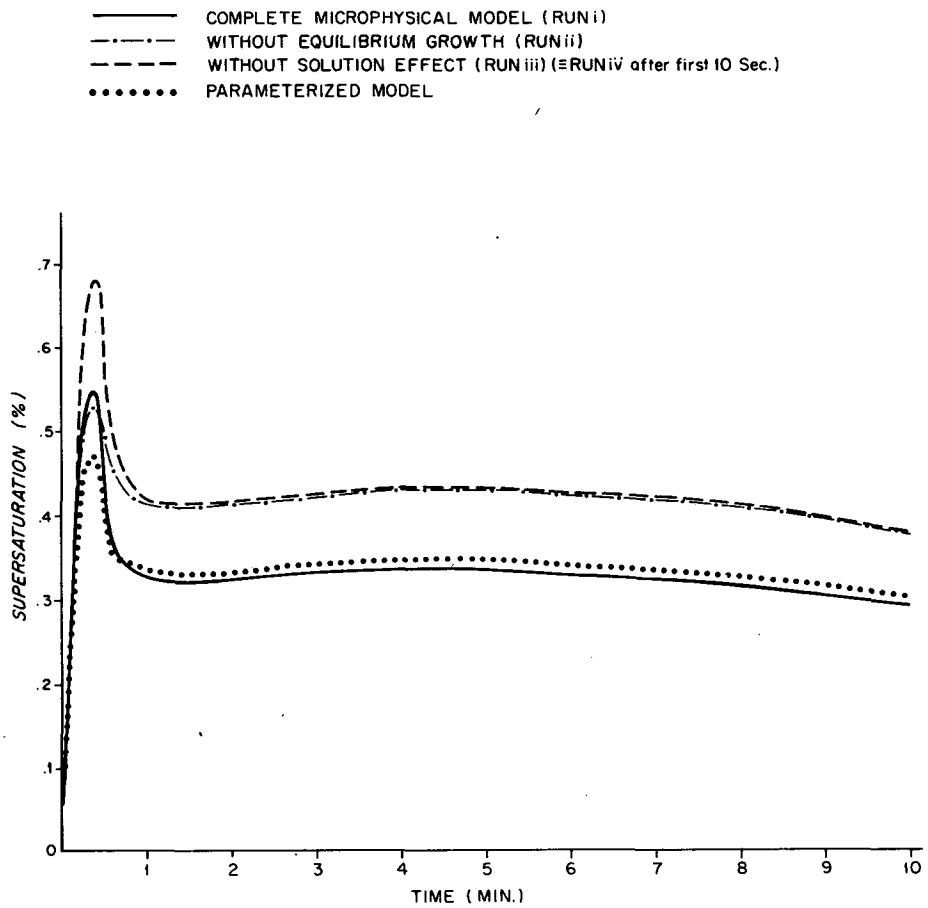

FIG. 3. Comparison of supersaturation predictions for the test runs (i)–(iv). See Section 3 of text for explanation.

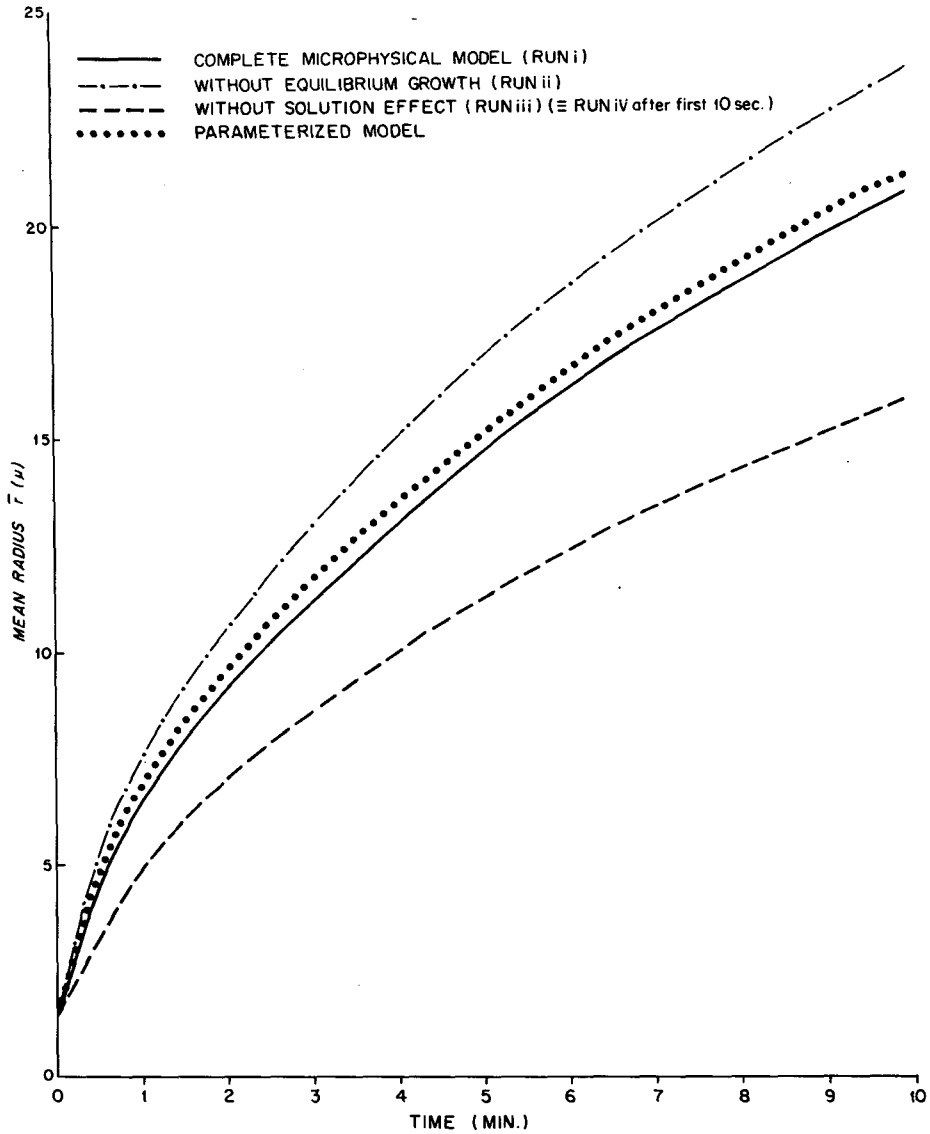

FIG. 4. Mean radius growth for test runs (i)–(iv).

results of runs (iii) and (iv) are identical except for the first 10 s indicates that equilibrium growth is not significant to the overall droplet growth while the solution term is ignored. In the next paragraph the importance of the equilibrium growth with the solution term retained [runs (i) and (ii)] will be stressed. The behavior of $(H_2 d\rho_w/dt)$ term in the S equation for runs (i)–(iv) as a function of time for the first minute of simulation together with the contribution from the equilibrium part to the liquid water change (shown in Fig. 5) reveals that the contribution from the first term in Eq. (7) is quite small and can be omitted without affecting the computations in run (i).

When equilibrium growth is neglected, the droplet radius is kept at its initial size until S exceeds the critical supersaturation S_c. Once S exceeds S_c, the growth rate of this droplet is governed by Eq. (3). The growth rate of this droplet becomes very large since the radius of this droplet is still in the submicron range and the contribution from the solution term is inversely proportional to radius raised to the fourth power. This feature can be seen from the sudden rising of $H_2 d\rho_w/dt$ at 3 and 6 s in Fig. 5 during the activation stage. This increase of $H_2 d\rho_w/dt$ contribution therefore produces a decrease of S [see Eq. (6) and Fig. 3] and in turn results in a smaller S_{max} in run (ii). Due to a decrease in S_{max}, the radius of the smallest activated droplet is 0.18 μm instead of 0.085 μm in runs (i) and (iii) which have a higher S_{max}. Thus, a fewer number of categories are acti-

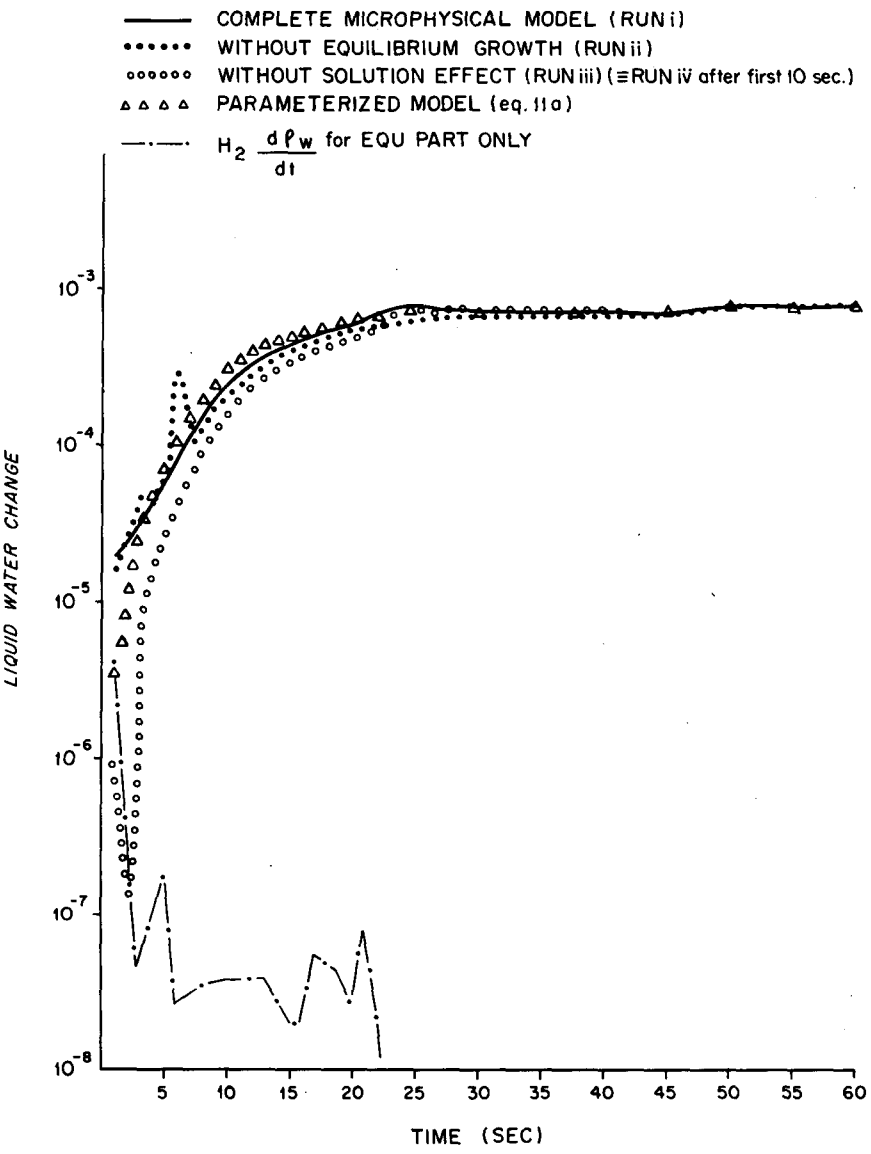

FIG. 5. Microphysical contribution to supersaturation prediction [second term on right-hand side in Eq. (5)] for test runs (i)–(iv).

vated in addition to initially large growth rate. This results in larger $\bar{r}$ in run (ii) than in the other runs as seen in Fig. 4. During the post-activation stage ($t>30$ s), $H_2 d\rho_w/dt$ in run (ii) decreases as a result of large $\bar{r}$. This produces a slow decrease in S and results in higher value of S than that of run (i) in the postactivation stage. It appears that the major factor in the difference between run (i) and run (ii) is Eq. (2) and not the $\sum_{EQU}$ term in (7).

Due to neglect of positive contribution from the solution effect in Eq. (6), S_{max} for run (iii) reaches ~30% higher than run (i). The droplet growth is reduced because of lack of contribution from solution term. This results in smaller $\bar{r}$, as seen in Fig. 4, even though the supersaturation is high (Fig. 3).

The above experiments have clearly demonstrated the significance of the equilibrium growth and solution terms. Despite their negligible magnitudes during the post-activation stage, during the activation stage the errors through the neglect of these terms are transmitted to the mean radius growth and the consequent results seem to diverge with time from the complete microphysical computation (see Fig. 4). This implies that the parameterization of the condensation process should retain complete microphysics implicitly or explicitly, especially during the activation stage.

4. Parameterization of the condensation process

The objective of this parameterization is to simplify the set of microphysical equations in such a way

that whatever the initial conditions may be, the parameterized equations are able to represent the basic features of the exact equations.

a. Equation for the supersaturation

From Eqs. (6) and (7) together with the fact that latent heat released due to equilibrium growth [proportional to the first term of Eq. (7)] can be neglected, Eq. (5) becomes

$$\frac{dS}{dt}=H_1W-H_2 4\pi\rho_l \sum_{\text{NEQU}} \Delta N r^2 \frac{dr}{dt},$$

which can be rewritten with the help of (4) as

$$\frac{dS}{dt}=H_1W-H_3 \sum_{\text{NEQU}} \left(Sr-a+\frac{b}{r^2}\right)$$

or

$$\frac{dS}{dt}=H_1W-H_3\left(S\bar{r}-a+\frac{\bar{b}}{\bar{r^2}}\right)N_1, \tag{10}$$

where $H_3=4\pi\rho_l G H_2$, N_1 is cumulative number density of activated nuclei, and the overbar is defined as

$$\bar{(\ )}=\frac{1}{N_1}\sum_{\text{NEQU}}(\ )\Delta N.$$

The complexity of the solution term poses a major difficulty in parameterizing Eq. (10). However, the behavior of the terms $(S\bar{r}-a+\overline{b/r^2})$ and $(S\bar{r}-a)$ shown in Fig. 6a reveal that the two terms differ only during the first 7 s of simulation. An assumption is thus made that the solution term can be omitted

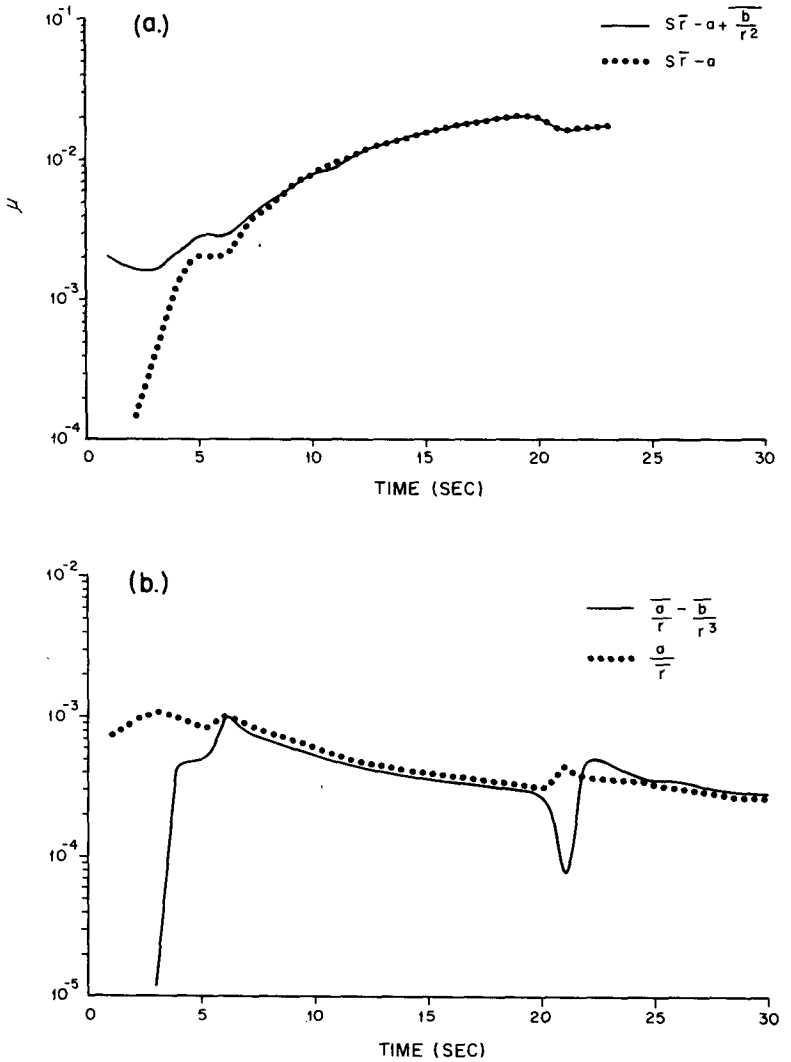

FIG. 6. Comparison (a) between terms $(S\bar{r}-a+\overline{b/r^2})$ and $(S\bar{r}-a)$ and (b) between terms $(\overline{a/r}-\overline{b/r^3})$ and $(a/\bar{r})$.

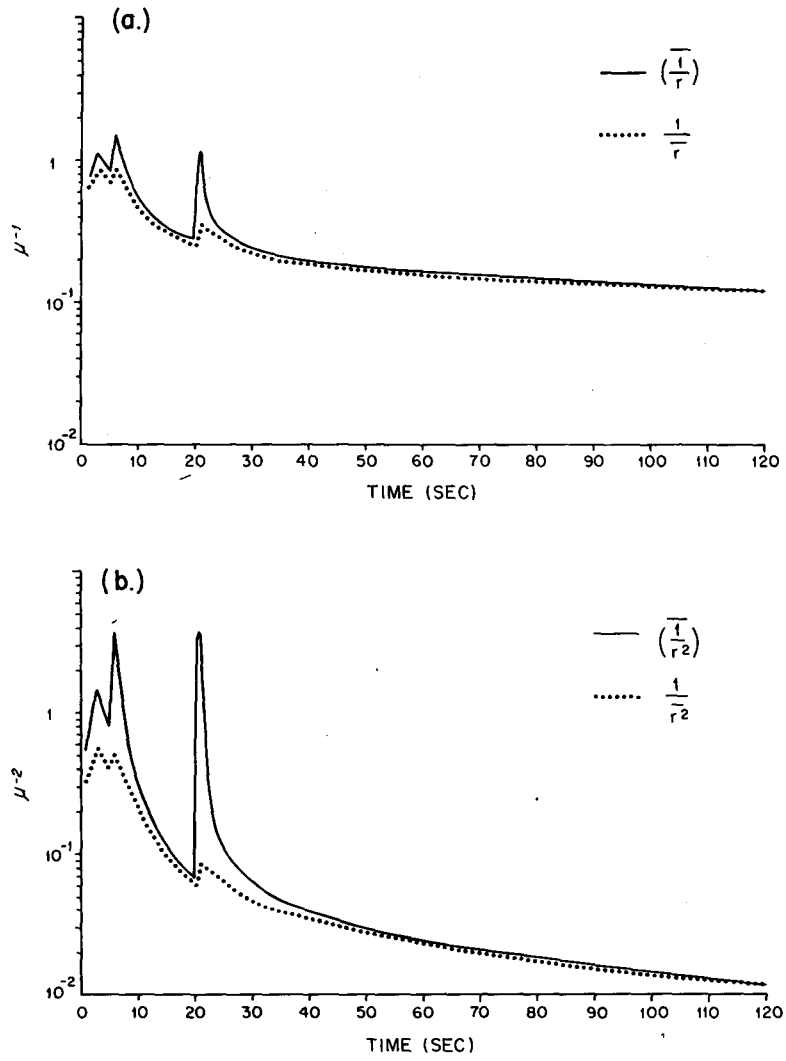

FIG. 7. Comparison (a) between $\overline{r^{-1}}$ and $(\bar{r})^{-1}$ and (b) between $\overline{r^{-2}}$ and $(\bar{r^2})^{-1}$.

in the first-order approximation. Eq. (10) becomes

$$\frac{dS}{dt}\approx H_1W-H_3(S\bar{r}-a)N_1 \text{ for all } t>0. \quad (11)$$

b. Equation for the first moment of the droplet distribution

To simplify the mean radius growth Eq. (9), the behaviors of 1) $\overline{r^{-1}}$ and $(\bar{r})^{-1}$, and 2) $\overline{r^{-2}}$ and $(\bar{r^2})^{-1}$ are computed and the results are presented in Fig. 7. The sudden jumps observed at 3, 6 and 21 s are related to the activation of new categories. After 40 s of simulation it is clear that

$$\overline{r^{-1}}\approx(\bar{r})^{-1} \quad \text{and} \quad \overline{r^{-2}}\approx(\bar{r^2})^{-1}. \quad (12)$$

Since the solution effect can be disregarded after 40 s (see Fig. 2a), Eq. (9) can be restated as

$$\frac{d\bar{r}}{dt}\approx G\left(\frac{S}{\bar{r}}-\frac{a}{\bar{r^2}}\right) \quad \text{for} \quad t>40 \text{ s}. \quad (13)$$

(Note that S and a are not functions of droplet radius.)

For the first 40 s or during the activation stage, the comparison between the quantities $(\overline{S/r}-\overline{a/r^2}+\overline{b/r^4})$ and $(S/\bar{r}-a/\bar{r^2})$, shown in Fig. 2b, reveals the empirical relationship

$$\frac{\bar{S}}{r}-\frac{\bar{a}}{r^2}+\frac{\bar{b}}{r^4}\approx\frac{S}{\bar{r}}-\frac{a}{\bar{r^2}}, \quad (14)$$

except for the first 4 s. In view of this the two terms on the right-hand side of (14) no longer represent the

supersaturation and curvature effects only, but through an internal compensation by use of $(\bar{r})^{-1}$ and $(\overline{r^2})^{-1}$, they implicitly include the solution effect. The parameterized form of mean radius growth then becomes

$$\frac{d\bar{r}}{dt}=G\left(\frac{S}{\bar{r}}-\frac{a}{\overline{r^2}}\right) \quad \text{for all} \quad t>0. \tag{15}$$

c. Equation for the second moment of the droplet distribution

Eq. (4) can be written as

$$\frac{d\overline{r^2}}{dt}=2G\left(S-\frac{\bar{a}}{r}+\frac{\bar{b}}{r^3}\right). \tag{16}$$

Again for $t>40$ s, $\overline{r^{-1}}\approx(\bar{r})^{-1}$ from Fig. 7a and the solution term in (16) can be dropped. Since $(\bar{r})^{-1}<\overline{r^{-1}}$ for $t<40$ s, we believe by the same token as in Section 4b above that

$$-\left(\frac{\bar{a}}{r}\right)+\left(\frac{\bar{b}}{r^3}\right)\approx-\frac{a}{\bar{r}}. \tag{17}$$

The contribution of the solution term is again absorbed in the term $(-a/\bar{r})$. Fig. 6b lends support to this argument. Hence the parameterized form of Eq. (16) can be written as

$$\frac{d\overline{r^2}}{dt}=2G\left(S-\frac{a}{\bar{r}}\right) \quad \text{for all} \quad t>0. \tag{18}$$

d. Equation for the number density of activated droplets

Twomey (1959) suggested that the number of condensation nuclei active at percent supersaturation S is given by

$$n(S)=CS^k. \tag{19}$$

Actually, nuclei will not be activated until S reaches S_c, the critical supersaturation, which is a function of molarity. Eq. (19) is a good approximation to observational data only above a certain minimal value of S_c and does not necessarily apply to large and giant salt nuclei (radius >1 μm). The constants C and k are determined for a given nuclei distribution by a regression method. Then in the subsequent droplet growth by the parameterized scheme, the total number density N_1 of activated droplets is computed according to

$$N_1=CS^k \tag{20}$$

since the Lagrangian framework is employed. During the activation stage S and N_1 increase. When the supersaturation reaches its maximum, N_1 also reaches a maximum and, thereafter, N_1 is kept constant since no more droplets can be activated.

The initial conditions are given by

$$\bar{r}_0=\frac{1}{N_I}\sum rn(r)\Delta r,$$

$$\overline{r_0^2}=\frac{1}{N_I}\sum r^2n(r)\Delta r,$$

$$S_0=H_1W,$$

where $N_I=\sum n(r)\Delta r$ and the summations taken are for those categories for which $S_0\geqslant S_c(r)$. The micro- and macro-time steps and the form of vertical velocity are the same as those used in the microphysical computations. The parameterization scheme is tested for Warner's nuclei distribution (see Table 1) using $C=225$ and $k=0.62$.

The supersaturation and mean radius development for 10 min of simulation using Eqs. (11), (15), (18) and (20) shown in Figs. 3 and 4, respectively, indicate close agreement between the microphysical and parameterized computations despite an about 14% error in $S_{\max}$ prediction.

The changes in liquid water content computed from

$$H_2\frac{d\rho_w}{dt}=H_24\pi\rho_l\bar{r}^2\frac{d\bar{r}}{dt}N_1 \tag{21}$$

are identical to those computed from

$$H_2\frac{d\rho_w}{dt}=H_3(S\bar{r}-a)N_1. \tag{11a}$$

Although during first 20 s there is a difference between the microphysical and parameterized models (see Fig. 5), the future development of supersaturation based on Eqs. (21) or (11a) agrees very well with that computed from the microphysical model.

The performance of this parameterization scheme was also tested using a constant vertical velocity in Eq. (11). The results for $W=1$, 2, 4 and 5 m s^{-1} are comparable to those obtained from the microphysical model. The results of the variable draft profile are only included here since the motions within a cloud parcel are time-dependent. The applicability of the proposed parameterization scheme to other types of nuclei distributions and its limitations are described in the following section.

5. Applications and limitations

Eight different distributions are used to compare the results of evolution of S and $\bar{r}$ from the micro-

TABLE 2. Comparison between the results of the parameterized model and the microphysical model for different types of nuclei distributions. N_0 is the cumulative number of nuclei in a given distribution, R the smallest radius activated and N_1 the cumulative number of activated nuclei in a given distribution. S and $\bar{r}$ are the supersaturation and mean radius. The subscript p on any variable refers to that derived through the parameterized model. The numbers on the subscript indicate simulation time in minutes. The performance of the parameterization scheme is indicated under "Comments."

Variable	Eriksson $N_p=20.6S^{0.1745}$	Warner $N_p=225S^{0.62}$	Case 1 $N_p=800S^{0.7}$	Case 2 $N_p=1000S^{0.7}$	Case 3 $N_p=1400S^{0.7}$	Case 4 $N_p=900S^{0.2}$	Case 5 $N_p=900S^{0.5}$	Case 6 $N_p=900S^{0.}$
N_0 (cm^{-3})	23.3	323	1378	1722	2412	1051	1327	1811
$R(\mu m)$	0.044	0.085	0.18	0.18	0.18	0.34	0.34	0.18
N_1 (cm^{-3})	21.8	145	323	404	565	605	333	281
N_{1p} (cm^{-3})	21.6	138	334	401	530	681	467	288
$\Delta N_1(\%)=(N_1-N_{1p})/N_1$	+19.1	+7.4	−3.1	0.74	6.2	−12.6	−40.2	−2.5
$S_{max}(\%)$	1.15	0.547	0.332	0.311	0.275	0.183	0.270	0.356
S_p at $S_{max}(\%)$	1.30	0.449	0.278	0.255	0.222	0.220	0.247	0.276
$\bar{r}(\mu m)$ at S_{max}	8.3	2.85	1.88	1.73	1.43	1.91	2.20	1.93
$\bar{r}_p(\mu m)$ at S_p	8.9	4.13	2.61	2.49	2.32	2.00	2.33	2.88
$S_1(\%)$	1.09	0.322	0.197	0.174	0.148	0.139	0.192	0.213
$S_{p1}(\%)$	1.27	0.329	0.190	0.171	0.149	0.132	0.159	0.205
$\bar{r}_1(\mu m)$	10.8	6.49	5.14	4.77	4.22	4.20	5.11	5.38
$\bar{r}_{p1}(\mu m)$	11.6	6.87	5.26	4.95	4.52	4.14	4.70	5.56
S_3	1.02	0.328	0.201	0.176	0.146	0.140	0.197	0.219
S_{p3}	1.18	0.342	0.197	0.176	0.150	0.131	0.162	0.215
$\bar{r}_3$	19.9	11.3	8.78	8.15	7.27	7.14	8.70	9.20
$\bar{r}_{p3}$	21.4	11.7	8.77	8.25	7.53	6.91	7.84	9.23
S_6	1.02	0.328	0.200	0.175	0.143	0.137	0.197	0.219
S_{p6}	1.18	0.344	0.196	0.175	0.148	0.128	0.160	0.215
$\bar{r}_6$	28.5	16.2	12.5	11.6	10.4	10.1	12.4	13.1
$\bar{r}_{p6}$	30.7	16.6	12.4	11.7	10.6	9.78	11.1	13.0
S_{10}	0.91	0.292	0.178	0.155	0.127	0.130*	0.175	0.195
S_{p10}	1.05	0.307	0.175	0.156	0.132	0.123*	0.142	0.191
$\bar{r}_{10}$	36.6	20.7	1.60	14.8	13.3	11.7*	15.8	16.8
$\bar{r}_{p10}$	39.4	21.3	1.59	14.9	13.6	11.3*	14.2	16.7
Comment**	Fair ($\Delta\bar{r}$ increasing while ΔS is more or less unchanged)	Good (both $\Delta\bar{r}$ and ΔS remain unchanged)	Excellent	Excellent	Excellent	Good ($\Delta\bar{r}$ slowly increasing)	Fair (bad prediction of S_p while $\Delta\bar{r}$ increasing)	Excellent (both $\Delta\bar{r}$ and ΔS decreasing)

* These quantities represent 8 min simulation time, since the microphysical computations blew up at 10 min.

** Comments include response to values of $\Delta\bar{r}=|\bar{r}-\bar{r}_p|$ and $\Delta S=|S-S_p|$.

physical model (Section 2) and the parameterized model (Section 4). Two are the observed nuclei distribution by Eriksson (1959) and Warner (1969), and the others are generated by choosing various combinations of the constants C and k in Eq. (20). The value for k is kept constant and C is varied in three cases, while in the remaining three cases C is kept constant and k is varied. The cumulative number of nuclei in the range 0.011–1.08 μm is obtained from (20). Nuclei of radius >1.08 μm are obtained by modifying Warner's data. These distributions are listed in Table 1.

The results using these eight distributions are summarized in Table 2. Variables with subscript p refer to quantities derived from the parameterized model. For cases with $k>0.6$ and the quantity $\Delta N_1=(N_1-N_{1p})/N_1$ not exceeding 10%, excellent agreement between microphysics and parameterization is found (see last row in Table 2). This is not hard to understand since for these cases there are fewer large (radius between 0.3 and 1 μm) and giant (radius >1 μm) condensation nuclei, so that the supersaturation (S_{max}) is able to reach a higher value without water vapor being consumed fast, and in turn more nuclei categories can be activated.

Once the supersaturation S, mean droplet radius $\bar{r}$, and the total activated number density N are obtained through parameterization, changes in liquid water content can be derived from Eq. (21). Also, since the warming of the bulk air by released latent heat and the total amount of supported liquid water are the only feedback effects from the condensation process on mesoscale dynamic processes, the parameterization scheme can be used to predict the change in the potential temperature as

$$\frac{d\theta}{dt}=\frac{\theta_0 L}{C_p T_0}\frac{dq_w}{dt}. \tag{22}$$

On the other hand, vorticity is influenced by the total liquid water content which serves as a sink. The vorticity equation is written as

$$\frac{d\zeta}{dt}=g\frac{\partial}{\partial x}\left(\frac{\theta_v'}{\theta_{v,0}}-q_w\right). \tag{23}$$

It is apparent that the macrophysical parameters (θ,ζ) can now be predicted through this simple pa-

rameterized microphysics. Furthermore, this can be applied to include the supersaturation effects in Kessler's (1969) parameterization. This may be achieved by replacing the temperature and vorticity equations of Kessler's scheme by Eqs. (22) and (23), respectively, and by using (11) to predict the supersaturation. Since coalescence changes the droplet distribution, this scheme is strictly applicable to nonprecipitating shallow cumuli.

6. Conclusions

The proposed parameterization for the condensation phase in cloud development successfully simulates the droplet growth due to condensation. The scheme is applicable to a variety of nuclei distributions, ranging from extreme maritime (Eriksson) to maritime-continental. Since the logic of this parameterization scheme is based on the behavior of the microphysics, it does not require that the initial droplet distribution possess an analytical form *a priori*. The proposed scheme successfully bridges the gap between condensation nuclei and cloud parameters, and can thus be used to approximate the interaction between the micro- and macrostructures of cumulus clouds.

Acknowledgments. The authors wish to extend their gratitude to Professor Geirmundur Árnason who initiated this investigation and provided valuable guidance throughout. The authors are grateful to Dr. James Jiusto for his helpful comments on the manuscript. Thanks are also extended to Miss Sally Young for typing the manuscript and to Mrs. Carol Clas for drafting the diagrams.

This research was supported by the Atmospheric Sciences Section of the National Science Foundation under Grants A0-32330-X02 and DES 75-13450.

APPENDIX

List of Symbols

These symbols either occur repeatedly or are not defined in the text. A subscript 0 is used to designate the environmental variables and a subscript p represents that variable derived through parameterization.

- a quantity proportional to the inverse of the temperature occurring in the droplet-growth equation
- b quantity proportional to the mole fraction of a salt nucleus occurring in the droplet-growth equation
- C coefficient in the relation between nuclei available for nucleation and supersaturation
- C_p specific heat per unit mass at constant pressure
- D diffusion coefficient of water vapor in air (0.226 cm^2 s^{-1}).
- F ventilation factor
- G function occurring in the droplet-growth equation
- g acceleration of gravity (981 cm s^{-2})
- H_1, H_2 functions in the prediction equation for supersaturation.
- i Van't Hoff factor
- k quantity occurring in the equation relating the nuclei available for nucleation and supersaturation
- l factor inversely proportional to the accommodation coefficient
- L latent heat of evaporation (2.50×10^{10} ergs g^{-1})
- m mass of dry salt nucleus
- M molecular weight of salt
- N_0 cumulative number density per unit volume in a given spectrum
- N_1 cumulative number density per unit volume of activated nuclei in a given spectrum
- ΔN number of nuclei or droplets per unit volume within a radius interval Δr
- ΔN_1 percentage difference in total number density between parameterized and microphysical models $[=100(N_1-N_{1p})/N_1]$
- n number of nuclei or droplets per unit volume per unit radius interval
- q_s saturation mixing ratio
- q_w specific water content (ρ_w/ρ_0)
- R_v gas constant for moist air (2.87×10^6 ergs g^{-1} K^{-1})
- r droplet radius
- r_0 radius of droplet at initial time
- r_c critical drop radius $[=(3b/a)^{\frac{1}{2}}]$
- $\bar{r}, \bar{r}^2$ first and second moments of nuclei distribution
- S supersaturation
- S_0 supersaturation at initial time
- S_c critical supersaturation $[=2a/3r_c]$
- T temperature (K)
- t time
- W vertical wind component
- x horizontal coordinate
- ζ vorticity for two-dimensional flow
- θ potential temperature
- θ_v virtual potential temperature
- θ_v' virtual potential temperature of the perturbation
- ρ density of air
- ρ_l density of liquid water
- ρ_v density of water vapor
- $\rho_{v,s}$ saturation density of water vapor
- ρ_w total liquid water content per unit volume.

REFERENCES

Árnason, G., and P. S. Brown, Jr., 1971: Growth of cloud droplets by condensation: A problem in computational stability. *J. Atmos. Sci.*, **28**, 72–77.

——, and R. S. Greenfield, 1972: Micro- and macro-structures

of numerically simulated convective clouds. *J. Atmos. Sci.*, **29**, 342–367.

——, —— and E. A. Newburg, 1968: A numerical experiment in dry and moist convection including the rain stage. *J. Atmos. Sci.*, **25**, 404–415.

Clark, T. L., 1973: Numerical modeling of the dynamics and microphysics of warm cumulus convection. *J. Atmos. Sci.*, **30**, 857–878.

——, 1974: A study in cloud phase parameterization using the gamma distribution. *J. Atmos. Sci.*, **31**, 142–155.

Eriksson, E., 1959: The yearly circulation of chloride and sulfur in nature: Meteorological, geochemical, and pedological implications. Part I. *Tellus*, **11**, 375–403.

Fletcher, N. H., 1966: *The Physics of Rain Clouds*. Cambridge University Press, 390 pp.

Kessler, E., 1969: On the distribution and continuity of water substance in atmospheric circulation. *Meteor. Monogr.*, No. 32, Amer. Meteor. Soc., 84 pp.

Rooth, C., 1960: A statistical study of cloud droplet growth by condensation. *Physics of Precipitation, Geophys. Monogr.*, No. 5, Amer. Geophys. Union, 220–224.

Silverman, B. A., and M. Glass, 1973: A numerical simulation of warm cumulus clouds: Part. I. Parameterized vs. non-parameterized microphysics. *J. Atmos. Sci.*, **30**, 1620–1637.

Twomey, S., 1959: The nuclei of natural cloud formation. II. The supersaturation in natural clouds and the variation of cloud droplet concentration. *Geofis. Pure Appl.*, **43**, 243.

Warner, J., 1969: The microstructure of cumulus cloud. Part II. The effect on droplet size distribution of the cloud nucleus spectrum and updraft velocity. *J. Atmos. Sci.*, **26**, 1272–1282.